2024 IEEE/RSJ International Conference on Intelligent Robots and Systems (IROS)
October 14-18, 2024. Abu Dhabi, UAE

TRX-Hand5: An Anthropomorphic Hand with Integrated Tactile Feedback for Grasping and Manipulation in Human Environments

Sicheng Yang, Wang Wei Lee, Zhong Zhang, Youda Xiong, Jiaming Liang, Peng Lu, Yonghui Zhu, Tianliang Liu, Jingchen Li, Rui Wang, Xiong Li, and Yu Zheng*, *Senior Member, IEEE*

***Abstract*— Objects of daily life are designed to suit the human hand. Without major modifications to these objects and our environments, robots will need end-effectors with human hand-like configuration and dexterity to efficiently operate on them. Tight integration of tactile and proprioceptive sensors are also critical to ensure robust execution of manipulation policies without sacrificing range-of-motion. Reliability is also key, and a mechanically robust, easy to repair end-effector is important to minimize downtime. To meet these challenges, we designed a 13 degree-of-freedom anthropomorphic hand with over 1000 tactile sensing elements, named TRX-Hand5. Also embedded within are positional encoders and cable tension sensors to provide proprioceptive perception. TRX-Hand5 has a novel biomimetic topology with six small posture motors in the palm to replicate the function of intrinsic hand muscles and five large power motors in the forearm to play the role of forearm flexor muscles. The whole hand weighs 2.6 kg with its dimensions comparable to those of an adult male's hand and is capable of actuating its fingertips at over 200°/s while exerting up to 22 N of force. The system can be disassembled in modules for easy maintenance.**

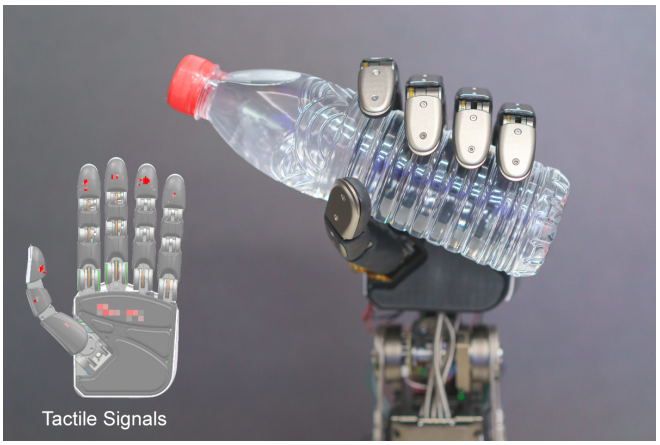

Fig. 1. TRX-Hand5 grasping a bottle of water. The inset shows the pressure distribution recorded by the integrated tactile sensors, where a higher color intensity indicates a higher pressure.

I. Introduction

The human hand is one of the most versatile and precise mechanical and sensory appendages in the biological world. Not only does it possess a remarkable 22 degrees of freedom (DoFs) [1], the strength and the speed at which the fingers can be actuated remain an elusive benchmark for roboticists to emulate. Equally as impressive is the sensing capabilities of the hand. Besides the ability to sense temperature and pain, glamorous skin of the human hands are densely innervated with four distinct mechanoreceptors that react to pressure, vibration, skin-stretch, and pressure changes [2]. These capabilities allow the human hand to not only serve as a tool for manipulation but also as an exploratory instrument that supplements our other sensing modalities.

For over a century, roboticists have endeavored to replicate the function and form of the human hand [3]. This approach is logical, as most objects in our living environments are designed for manipulation by the human hand. Therefore, robots intended to handle the same objects should ideally be equipped with an end effector of a similar configuration and dexterity. However, the technology and mechanisms available to robots are fundamentally different from those that living organisms have evolved to depend on [1]. Notably, current artificial hands primarily rely on electric actuators that cannot yet match the power density provided by biological muscles [4]. Consequently, compromises on dexterity, weight, dimension, and speed are unavoidable when designing an anthropomorphic hand.

In scenarios where human-like dexterity is not essential, a common and practical approach is to reduce the hand's DoFs, relying instead on underactuated mechanisms to achieve compliance and easy control [3]. The advantage of an underactuated design is that very few motors are required, making the hand lightweight, robust, power-efficient and economical [5]–[8]. However, precise manipulation becomes challenging to achieve as the passive joints are inherently uncontrollable.

On the other hand, there are artificial hands that strive to match the dexterity of human hands, such as MIT/Utah hand [9], Shadow Hand [10], DLR/HIT Hand II [11], KITECH-Hand [12], NASA Robonaut hand [13], and others [3]. As each DoF uses an individual actuator, these hands are typically larger, heavier, and significantly more complex. To retain the slim and light profile of the palm and fingers, most designs place the actuators in the forearm [10], [13], [14], necessitating the routing of numerous cables through the wrist. This further increases system complexity and limits its practicality and ease of repair.

Over the years, many robotic hands featuring various configurations have been developed. However, the integration of tactile sensing capability has only gained momentum recently [15]. Integrating sensors, readout circuits, and communication electronics into a robust and compact mechanical system is no easy task, even though mechanisms for transducing contact forces are well known [16]. There are demanding constraints to consider, such as a wiring scheme that does not

All the authors are with Tencent Robotics X, Shenzhen, Guangdong 518057, China.
*Corresponding author (E-mail: petezheng@tencent.com)

interfere with finger movement and custom-shaped sensor patches that follow the contour of the fingertips [17].

The applicability of a particular tactile sensing modality in anthropomorphic hands heavily depends on the possibility of miniaturizing the technology. For example, high-precision multi-directional load cells can only be installed at selected locations in limited numbers due to the restricted space in the fingers [18], [19]. Meanwhile, popular vision-based tactile sensors have mostly been installed on soft and/or bulky grippers with limited degrees of freedom, given the space requirements of the optical system [20]–[22].

Despite these challenges, there have been commendable efforts to integrate tactile sensing onto anthropomorphic hands. Notable examples include the Robonaut 2 hand with custom multi-directional load cells [13], Gifu Hand III with a custom piezoresistive sensing array [23], Shadow Hand with SynTouch Biotac [24], iCub hand with custom capacitive sensor patches [17], and Allegro hand with Uskin [25].

This paper presents TRX-Hand5, a robust, easily repairable robotic hand similar in size and configuration to the human hand. The hand is aimed at manipulating everyday objects in uncontrolled environments. Although bio-mimicry is not our main focus, one key design concept is the bio-inspired actuator layout, where larger brushless motors in the forearm provide greater power for grasping while smaller motors in the palm control precise positioning. This approach offers three main advantages: it contributes to enhancing the payload and velocity, simplifies cable routing through the wrist for easy repairs and replacements, and allows for modular self-contained finger assemblies. Custom curved tactile sensor arrays cover the fingertips, inner phalanges, and palmar surfaces to enhance contact awareness. Tension gauges integrated in the forearm monitor the tension of the primary cables, while joint encoders installed on all active joints facilitate precise manipulation.

The main contributions of our work are as follows:

1) A new multi-DoF anthropomorphic hand with integrated tactile sensor arrays is proposed;
2) A new design concept is implemented, where large power actuators are situated in the forearm while modular finger assemblies with fine cooperative posture actuators reside in the palm of the hand;
3) The performance of our prototype is characterized;
4) We also demonstrate how to integrate the tactile and tension sensing elements while maintaining the compactness of the design.

The paper is organized as follows. Section II describes the key constraints considered and the design decisions taken. Section III elucidates the mechanical design, electrical and sensing electronics. Section IV highlights the key achieved performance metrics. Section V concludes the paper.

II. Design Philosophy

TRX-Hand5 is aimed at providing a practical and efficient end-effector, enabling robots to share tools and environments with humans seamlessly. To this end, TRX-Hand5 is necessitated to exhibit the following characteristics: sufficient dexterity, anthropomorphic dimensions, practical payload and speed performance, extensive faculties for tactile, force and positional perception, as well as exemplary reliability and maintainability. This section describes the design decisions made to address these factors.

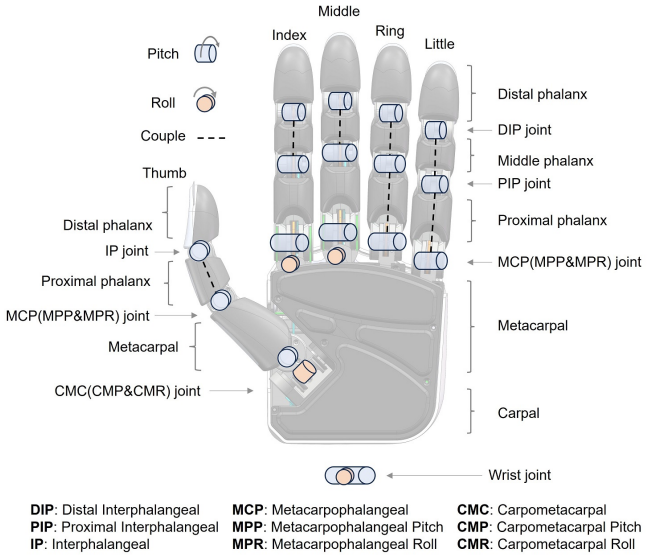

Fig. 2. Configuration design of TRX-Hand5.

A. Configuration Design

Like its biological counterpart, TRX-Hand5 should fulfil the three main functions, i.e., object grasping, non-prehensile interactions and dexterous manipulation. Dexterous manipulation has the most stringent requirements, since it requires the hand to satisfy the following two conditions:

1) When a finger joint is moved, it should induce arbitrary motion in the object.
2) When all finger joints are fixed, motion of the object should be fully restrained.

Using a hand-object system described in [26], we determine that a minimum of 3 fingers, each with 3 DoFs, is needed to meet the two conditions. Assuming that these fingers are the thumb, index, and middle fingers, the dexterity of the ring and pinky fingers can be simplified accordingly.

Another popular method to study hand configurations is to observe how the human hand is often used, systematically categorizing the different poses into a taxonomy [27]. One widely used taxonomy is the Feix taxonomy [28], which classifies the grasping patterns of the human hand into 33 types. We observe that only 4 patterns require active participation of the ring and pinky fingers. For other grasps, however, they are primarily used to increase contact points for enhancing stability and load capacity. Thus, we posit that a simplified finger design with 1 DoF should be sufficient for the ring and pinky fingers.

Figure 2 illustrates the configuration proposed for TRX-Hand5, with the thumb, index, and middle fingers having 3 DoFs each and the ring and pinky fingers having 1 DoF each, resulting in a total of 18 joints and 11 DoFs.

B. Payload and Velocity

The appropriate payload and speed hold considerable importance for the practicality of robotic hands in human living environments. Although fingertip forces of up to 80 N have been documented for human hands, a majority of individuals struggle to consistently exert 20 N for a minute using their fingertips [29]. Furthermore, items commonly used in daily life typically weigh less than 1 kg [30]. Consequently, we deduce that a fingertip force of 10 N should be necessary for most domestic scenarios.

The average finger velocity of the human hand is about 172°/s when performing daily tasks [29]. While finger velocity directly affects manipulation efficiency, we contend that as long as this velocity is not substantially compromised, there should not be a noticeable impact on the performance of anthropomorphic robotic hands in daily use.

At present, the majority of dexterous robotic hands are actuated by electric motors. The payload and velocity of motor-driven dexterous hands primarily depend on the motor's power, which is directly correlated to its size. Since electric motors possess limited power density compared to human musculature, constructing an anthropomorphic hand with dimensions akin to a human hand will significantly restrict its overall payload and velocity. To overcome this constraint, various motor arrangements have been explored by roboticists when designing dexterous hands. Common topologies include:

1) Housing all motors within the hand: This facilitates modular design but is the most space-constrained. To obtain a practical payload and velocity, a trade-off between the DoFs and the size of the hand is unavoidable.
2) Placing all motors externally, typically in the forearm: This method allows for the incorporation of more and larger motors, enhancing performance while maintaining a slender and lightweight hand. However, striving to concurrently attain high DoF and practical performance often results in a bulky and heavy forearm, limiting its applicability on mobile operation platforms. Moreover, the increased complexity of the drive mechanisms may reduce the system's repairability.
3) Mixed arrangement of motors, with some in the hand and others in the forearm: This bio-inspired strategy optimizes the utilization of both intra-hand and extra-hand space. Models such as the RoboRay Hand [31] and the iCub Hand [32] employ this approach to accomplish high dexterity without an oversized forearm. Nonetheless, this technique may lead to an increase in complexity and significant maintenance challenges, and thus is less popular.

Through extensive examination into the mechanics of human hand motion, we observe that muscles housed within the palm and those situated in the forearm contribute approximately equally to this function. Despite their diminutive size, the intrinsic muscles within the palm are pivotal in achieving dexterous manipulation using the fingers. For example, the interosseous muscles embedded in the palm primarily control

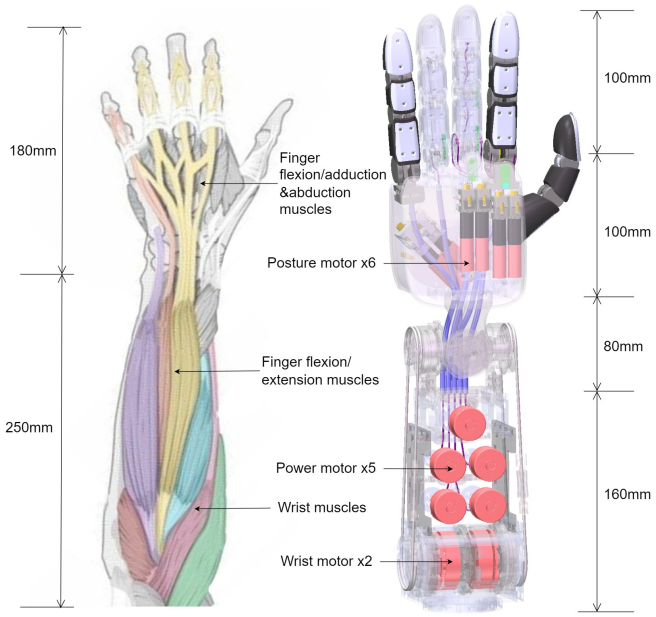

Fig. 3. Comparison of the human hand and TRX-Hand5.

finger abduction and adduction. The interosseous, lumbricals and forearm flexor muscles all contribute to finger flexion, whereas larger forearm muscles are the main source of strength when grasping heavy objects [33].

Guided by these insights, we propose a novel biomimetic topology, as shown in Fig. 3. We position six small posture motors within the palm to replicate the function of intrinsic hand muscles, while five large power motors installed within the forearm play the role of forearm flexor muscles. We did not implement forearm extensor muscles, opting instead to use springs in the palm to achieve finger extension, thus reducing the complexity of the system. Located at the bottom are two larger motors that control the wrist through cable transmission, thereby situating the system's center of gravity as close to the forearm as possible.

C. Sensors

Besides having sufficient dexterity, complex manipulation and proficient grasping necessitate robust tactile perception. The human hand boasts the greatest concentration of mechanoreceptors in the human body [2], underscoring the importance of tactile feedback in daily utilization. Given that the objective of TRX-Hand5 is to attain dexterous manipulation on par with human capabilities, it must be designed to seamlessly incorporate tactile sensors across the broadest range of contact surfaces feasible. Moreover, all joint angles should be monitored in real-time to enable accurate manipulation.

D. Reliability and Maintainability

Serving as end effectors for robots, dexterous hands will make frequent physical interaction with the external environment and are anticipated to operate in complex, unstructured settings where unforeseen collisions are likely to occur. Consequently, TRX-Hand5 should exhibit adequate resilience to

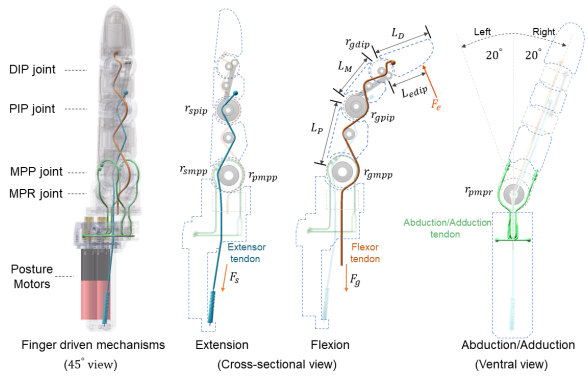

Fig. 4. Design of the manipulation finger.

minor collisions, while components prone to wear and tear must be designed for easy replacement.

III. Electromechanical System Design

A. Overview

TRX-Hand5 measures 95×80×442 mm^3 and weighs 2.6 kg. Its five fingers are composed of three unique designs, namely a 3-DoF thumb, 3-DoF index and middle fingers, and 1-DoF ring and pinky fingers. Mounted on a 2-DoF wrist, TRX-Hand5 can support up to 7 kg and offer a joint velocity of over 200°/s. The hand also features a suite of tactile and proximity sensors as well as joint encoders and cable tension monitors.

B. Finger Design

The majority of parts are shared between the thumb, index, and middle fingers. While the index and middle fingers are identical, the thumb differs in length and posture motor placement. Each of the three fingers has 3 DoFs, collectively referred to as manipulation fingers, as shown in Fig. 4. The index and middle fingers measure 104 mm from the MPP to the fingertip, with a width and depth of approxmiately 20 mm. These dimensions bear a close resemblance to those of an average human digit. Hall encoders are installed in MPR, MPP, and PIP joints to directly measure the joint angles, and the PIP and DIP joints are coupled by linkages.

The MPP and MPR joints of the manipulation fingers are driven differentially using abuction/adduction tendons by two posture motors. The DIP and PIP joints are actuated by motor modules in the forearm via flexor tendons. Each module consists of a brushless motor and a micro harmonic drive. In particular, the flexor tendon can also distribute torque to the MCP joint for greater fingertip force.

To achieve independent control of each joint and maximize fingertip force, the radii $r_{g_{\text{pip}}}$ and $r_{g_{\text{dip}}}$ of the flexor tendon at PIP and DIP joints are optimized as

$$
\begin{aligned}
\max_{r_{g_{\text{pip}}}, r_{g_{\text{dip}}}} \quad & \alpha F_e(\theta_{\text{mpp}} = 0°, \theta_{\text{pip}} = 0°) + \\
& \beta \min_{\theta_{\text{pip}}, \theta_{\text{mpp}} \in [0°, 90°]} F_e(\theta_{\text{mpp}}, \theta_{\text{pip}}) \\
\text{s.t.} \quad & \\
& F_s r_{s_{\text{mpp}}} + F_e L_{e_{\text{mpp}}} - F_g r_{g_{\text{mpp}}} - 2F_p r_{p_{\text{mpp}}} = 0 \\
& F_s r_{s_{\text{pip}}} + F_e L_{e_{\text{pip}}} - F_g r_{g_{\text{pip}}} + T_{\text{linkage}\to\text{pip}} = 0 \\
& F_e L_{e_{\text{dip}}} - F_g r_{g_{\text{dip}}} + T_{\text{linkage}\to\text{dip}} = 0 \\
& 0 \le F_g \le \frac{T_{\text{grasp\_motor}}}{r_{\text{grasp\_motor}}} \\
& -\frac{T_{\text{posture\_motor}}}{r_{\text{p\_r\_motor}}} \le F_p \le \frac{T_{\text{precision\_motor}}}{r_{\text{p\_r\_motor}}} \\
& L_{e_{\text{pip}}} = L_{e_{\text{dip}}} + L_m cos(\theta_{\text{pip}}) \\
& L_{e_{\text{mpp}}} = L_{e_{\text{pip}}} + L_p cos(\theta_{\text{mpp}}) \\
& L_{\text{spring\_extension}} = r_{s_{\text{pip}}}\theta_{\text{pip}} + r_{s_{\text{mpp}}}\theta_{\text{mpp}} \\
& F_s = F_{s\_\text{initial}} + kL_{\text{spring\_extension}}
\end{aligned}
\tag{1}
$$

where α and β are the weights of the corresponding objective terms. The term $F_e(\theta_{\text{mpp}} = 0°, \theta_{\text{pip}} = 0°)$ is the maximum fingertip force in the case that the finger is fully extended, while $\min F_e(\theta_{\text{mpp}}, \theta_{\text{pip}})$ is the smallest maximum force that can be exerted by the fingertip over different joint angles. F_g, F_p, F_s, and F_e represent the forces at the flexor tendon, abduction/adduction tendon, extensor tendon, and the fingertip, respectively. r_g, r_p and r_s are the winding radii of the flexor, abdunction/addunction, and extensor tendons, respectively, θ is the rotational angle, and L_e is the moment arm of the external force at the fingertip applied to respective joints as indicated by their subscripts. L_m and L_p are lengths of the middle and the proximal phalanges and $T_{\text{linkage}\to x} + F_s r_{s_x}$ corresponds to the coupling four-bar linkage's torque effect on the joint x. $L_{\text{spring\_extension}}$, F_{s_initial}, and k correspond to the initial extension, preload force, and elastic coefficient of the spring that is used to balance the weight of the finger and facilitate its rebound. When the finger flexes and the spring is stretched, a spring with small k is needed to maintain the spring resistance. However, the minimum value of k is constrained by the space. In this work, $k = 900$ N/m.

By evenly sampling $r_{g_{\text{dip}}}$ and $r_{g_{\text{pip}}}$ between $[2, 10]$ mm at intervals of 0.1 mm, we solve (1) and obtain the optimal values of $r_{g_{\text{dip}}} = 2.5$ mm and $r_{g_{\text{pip}}} = 7.5$ mm, which produces a theoretical maximum fingertip force of 21.9 N when fully extended. Figure 5 shows the computed maximum fingertip forces as the PIP joint angle is varied.

The maximum fingertip force at lower PIP joint angles is primarily limited by the forearm actuation motor module. At larger PIP joint angles, the forward external force applied to the fingertip generates a bending torque on the MPP joint, requiring posture motors to provide a reverse extension torque. However, since the posture motor's force is relatively small, the maximum fingertip force is reduced when the PIP joint's angle is larger. As the MPP joint's angle increases from 0° to 90°, by comparing Figs. 5a and 5b, it can be seen that the maximum fingertip force does not vary significantly

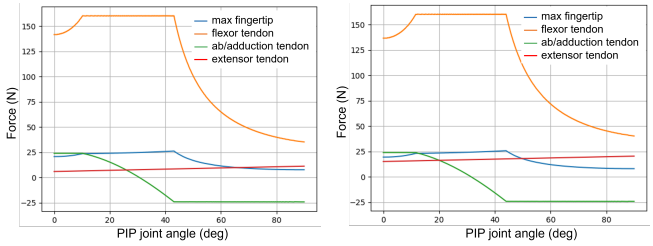

(a) (b)

Fig. 5. Computed forces of the fingertip, the flexor tendon, the extensor tendon and the abduction/adduction varies at different PIP joint's angles. (a) $\theta_{\text{mpp}} = 0°$. (b) $\theta_{\text{mpp}} = 90°$.

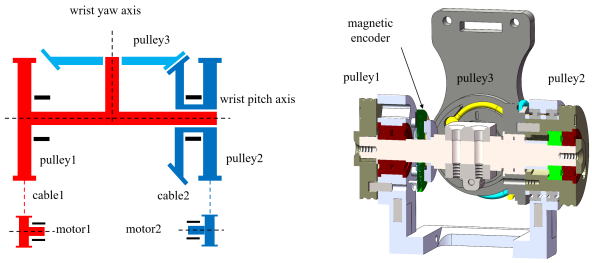

(a) (b)

Fig. 6. Illustration of (a) the wrist's movement mechanism and (b) the cross-sectional view of the specific mechanism.

at different PIP joint's angles, which is due to the relatively small elastic coefficient k of the spring.

The 3-DoF manipulation fingers feature a unique coupling mechanism between the 2 posture motors and a flexor tendon for increased output force. The actuation logic is as follows:

1) MPR joint abduction is achieved by rotating both posture motors clockwise at the same speed, while MPR joint adduction occurs when both motors rotate counterclockwise at the same speed.
2) MPP joint flexion/extension occurs when the posture motors rotate in opposite directions at the same speed. Relative differences in angular velocity between the two posture motors will cause simultaneous movement of the MPR and MPP joints.
3) The flexor tendon controls the flexion/extension of the PIP and the DIP joints. Within a certain tension range of the tendon, movements of the MPP and MPR joints are unaffected. However, if the MPR joint is moving, the tendon tension must be dynamically adjusted to maintain the posture of the PIP and DIP joints.

A proportional-derivative (PD) controller is developed to implement the logic described. The error term $e(k)$ for posture motors A, B and forearm tendon are as follows:

$$e(k)_{\text{A}} = -(\theta^t_{\text{mpp}} - \theta^n_{\text{mpp}})r_{p_{\text{mpp}}} + (\theta^t_{\text{mpr}} - \theta^n_{\text{mpr}})r_{p_{\text{mpr}}}$$

$$e(k)_{\text{B}} = (\theta^t_{\text{mpp}} - \theta^n_{\text{mpp}})r_{p_{\text{mpp}}} + (\theta^t_{\text{mpr}} - \theta^n_{\text{mpr}})r_{p_{\text{mpr}}}$$

$$e(k)_{\text{forearm}} = (\theta^t_{\text{mpp}} - \theta^n_{\text{mpp}})r_{g_{\text{mpp}}} - (\theta^t_{\text{pip}} - \theta^n_{\text{pip}})(r_{g_{\text{pip}}} + r_{g_{\text{dip}}})$$

where θ^t and θ^n are the target and current joint angles, and their subscripts denote the specific joints. $r_{p_{\text{mpr}}}$ is the winding radius of the abduction/adduction tendon at the MPR joint.

The 1-DoF grasping finger is much simpler, driven by only one flexor tendon, and thus not detailed in this paper.

C. Wrist Design

TRX-Hand5 features a 2-DoF coaxial wrist with large range of motion ($\pm 60°$ flexion/extension and $\pm 45°$ abduction/adduction). Two motor modules, each consisting of a micro harmonic drive and a brushless motor, actuate the wrist via a cable-driven differential drive. The rated torque of the two joints in the wrist can reach up to 8 Nm. Figure 6 illustrates the schematic diagram and cross-sectional view of the mechanism. The pulleys that are connected to the wrist motors by cables are placed on the outside of the wrist's fixed support. Meanwhile, the angular encoder is assembled inside the wrist's fixed support.

D. Design Modularity

Modular design can significantly enhance the reliability and maintainability of the dexterous hand. The 3-DoF manipulation finger module is essentially a self-contained unit with only one flexor tendon to be attached externally. Embedded within are two posture motors, an extension spring, four ab/adduction tendons, and one extensor tendon. Dyneema ropes with a diameter of 1 mm rated for 300 N are used for ab/adduction and extensor tendons. Given that the predicted maximum tension is only 30 N (Fig. 5), the high margin of safety should ensure the reliability of these internal tendons.

The flexor tendon, bearing the highest load and having the longest driving path among all tendons, sustains the highest risk of damage. To ensure its reliability, a 1.2 mm Dyneema rope rated for 500 N is selected. The transmission path was also optimized accordingly, with a combination of bearing guidance in the forearm and spring sleeve with PTFE tube in the palm and wrist segments to minimize wear and tear.

The modular concept extends throughout the design of TRX-Hand5, from the hand, wrist and forearm down to the flexion and wrist motors, facilitating quick disassembly and easy component replacement. We included a disassembly and cable replacement segment in the supplementary video to emphasize the modularity and repairability of TRX-Hand5.

E. Electrical System Design

Figure 7 depicts the block diagram of TRX-Hand5's electrical system, which is highly integrated and modular. The system accepts DC power supply from 32 V to 60 V. Control commands are relayed via EtherCAT at 4 kHz between the host PC and the Electrical Control Units (ECUs) in the forearm and palm, where they are translated to various other signals that directly control the 6 posture motors in the palm and 7 brushless motors in the forearm. The ECUs also sample joint encoders in the fingers and wrist at 1 kHz to achieve closed loop control. Key to the miniaturization of the ECUs is the use of the AX58400 System-On-Chip (SOC) with integrated dual-core processor and EtherCAT controller. Special care in component layout was also taken

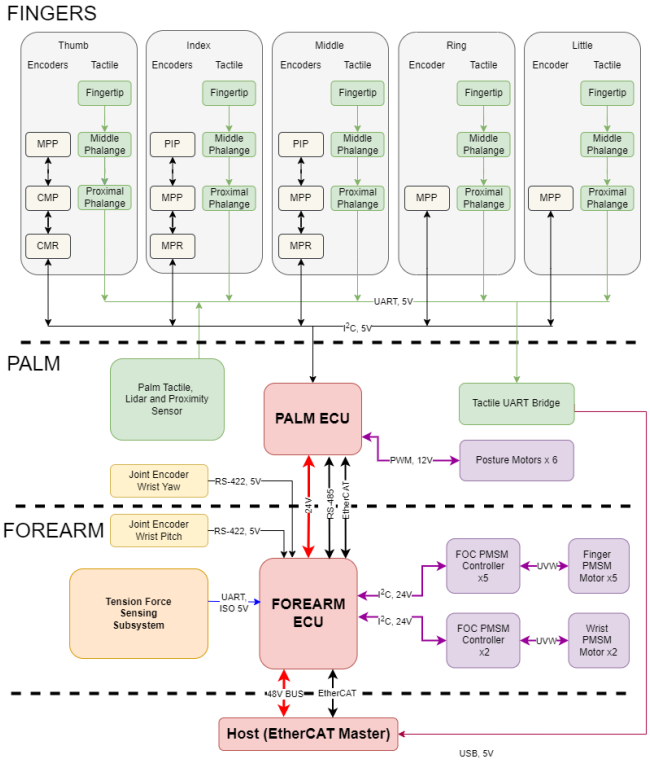

Fig. 7. Electrical system block diagram of TRX-Hand5.

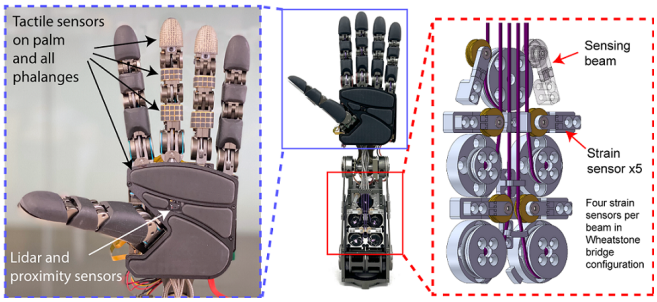

Fig. 8. TRX-Hand5 with a total of 1163 tactile sensing elements distributed across the palm and all finger phalanges. The palm also features lidar and proximity sensing. Strain gauges installed on the sensing beams monitor the tension of flexor tendons in the forearm.

to ensure optimal cable routing and easy maintenance within the limited space available.

F. Tactile and Proximity Sensing

TRX-Hand5 has a total of 1163 tactile sensitive elements, or taxels, fabricated as patches of sensor arrays that cover the fingertips, innerphalanges and palmar surfaces. The taxel distribution is non-uniform, with the fingertips having the highest spatial resolution at 1.1×1.1 mm^2 per taxel spaced 1.8 mm apart, while other surfaces feature 3×3 mm^2 taxels spaced 5 mm apart (Fig. 8). Notably, taxels on the fingertips were fabricated using our novel thermoforming method to conform to the ergonomically rounded curvatures essential for efficient manipulation [34]. The taxels are designed to be sensitive to pressure between 25 to 50 kPa. A total of 16 sensor patches are used, each having its own microcontroller for sampling and local processing of the piezoresistive elements at 100 Hz (Fig. 7).

TABLE I. Specifications of TRX-Hand5

Items		Parameters
Dimension		$95\times80\times442$ mm^3
weight		2.6 kg
Motors	Hand	6 posture motors (1 W)
		5 power motors (10 W)
	Forearm	2 wrist motors (40 W)
Fingertip force	Manipulation finger	22 N
	Grasping finger	11 N
Joint speed	MPR	300°/s
	MPP	220°/s
	PIP&DIP	300°/s
Tactile Sensors	Fingertip	156 taxels
	Innerphalanges (thumb)	54 taxels
	Innerphalanges (others)	45 taxels
	Palm	149 taxels
Proximity	Palm	8×8 LiDAR
		Infrared
Communication	Motors	EtherCAT
	Tactile	USB and UART

In addition, an 8×8 LiDAR array (VL53L5CX from STMicroelectronics) is situated at the center of the palm, next to an infrared transceiver pair (TEMT7100X01 and VSMY1850 from Vishay). The LiDAR provides accurate multi-zone distance measurements at 15 Hz, while the infrared transceiver delivers rapid readout of 125 Hz for objects within 10 cm range. These proximity sensors are used in tandem to achieve fast and accurate distance measurements between the palm and external surfaces.

A proprietary event-based protocol implemented via UART is used to transmit the sparse tactile and proximity data. Similar to the method in [35], the latest reading is updated only when a significant change in signal is detected, ensuring low latency and optimal use of communication bandwidth.

G. Tendon Tension Sensors

To measure the force applied to each finger, we incorporated tension sensing on all flexor tendons in the forearm. The tension of the flexor tendons are monitored by strain gauges installed on a cantilever beam (Fig. 8). Utilizing a classic Wheatstone bridge configuration, minor deflections of the beam caused by tension variations are transduced and amplified. The resultant signal is sampled at 500 Hz and relayed to the main controller via UART protocol. Experimental results demonstrate that the configuration achieves a tension resolution of 1 N within the range of 0 to 100 N, with a linearity of 97.06%.

IV. Performance Evaluation

To validate the performance of the proposed dexterous hand, we subjected TRX-Hand5 to rigorous testing procedures with emphases on peak fingertip force, joint speed, and dexterity. Its specifications and performance are summarized

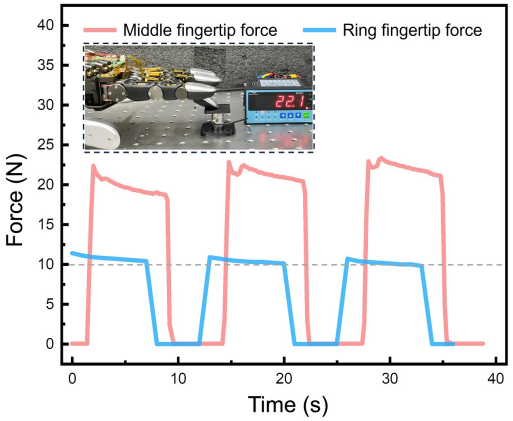

Fig. 9. Fingertip force test result of TRX-Hand5.

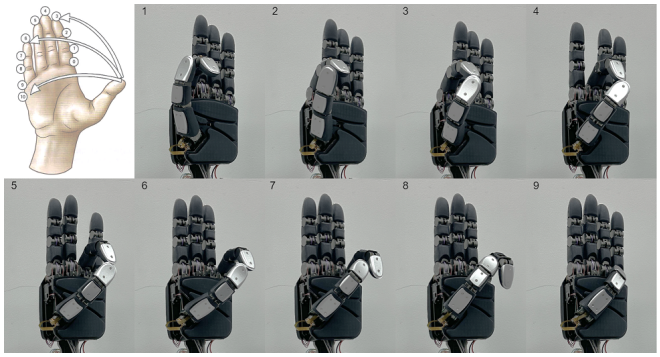

Fig. 10. Kapandji test result of TRX-Hand5.

in Table I. Various demonstrations of the proposed robotic hand are shown in the accompanying video.

The fingertip force is measured by pressing a force sensor using the fingertip of TRX-Hand5 from a horizontal pose (see Fig. 9). Peak forces of 22 N and 11 N were recorded for the 3-DoF manipulation fingers and 1-DoF grasping fingers, respectively, which are very similar to the computed maximum forces. Additionally, the MPR, MPP, PIP, and DIP joints were all observed to be capable of exceeding 200°/s, matching that of the average human hand when performing daily activities.

The synergistic movement effect of the thumb and other fingers plays a significant role in the dexterity of a hand, which can be verified by the Kapandji test [36]. In this test, the thumb is required to sequentially touch ten points on the other fingers and the palm. As shown in Fig. 10, TRX-Hand5 can achieve contact with the first nine points on the palm. Given that the tenth point is a difficult scenario even for the human thumb, we think that the impact of this deficiency on manual dexterity should be minimal.

Moreover, we used the Feix taxonomy [28] to evaluate the grasping ability of TRX-Hand5. A collage of all grasps is provided in Fig. 11, where TRX-Hand5 is shown to be able to execute all 33 types of grasps in the taxonomy, suggesting that it is well-adapted to handle everyday grasping tasks in human living environments.

The functionality and real-time performance of the tactile, proximity and tension sensors are demonstrated in the supplementary video.

V. Conclusion and Future Work

TRX-Hand5, a dexterous anthropomorphic hand with integrated tactile feedback for grasping and manipulation in human environments, is introduced. It possesses 11 DoFs in the hand and 2 DoFs in the wrist. Dexterous manipulation is achieved mainly using the 3-DoF thumb, index, and middle fingers while additional assistance in grasping is provided by the 1-DoF ring and pinky fingers. A biomimetic motor arrangement is also introduced, where the MCP joints of fingers are collaboratively driven by small posture motors within the palm that mimic the interosseous muscles, while five larger motors in the forearm replicate the finger flexor muscles, delivering strength for grasping heavy objects. TRX-Hand5 also features an extensive suite of sensors, with numerous tactile and proximity sensors covering the fingers and palm, angle encoders on all active joints, and tension sensors on the five flexor tendons. To facilitate easy maintenance and minimize downtime, TRX-Hand5 is designed in modules that can quickly be disassembled and replaced. A thorough evaluation of the durability and reliability of TRX-Hand5 over extended use will be conducted in the near future.

In an era where data-driven algorithms are rapidly evolving and increasingly deployed, there is a growing need for comprehensive manipulation datasets to drive the advancement of robotic manipulation in real-world settings. With dimensions akin to the human hand, TRX-Hand5 is intended to be a practical and dependable end-effector, furnished with an extensive suite of sensors for robots learning to explore the physical world and interact with real-life objects. We envision a future where robots are commonplace in every household, and expect that the concepts introduced in TRX-Hand5 will inspire future generations of anthropomorphic hands to work toward such a vision.

References

[1] L. A. Jones and S. J. Lederman, *Human hand function*. Oxford university press, 2006.

[2] R. S. Johansson and J. R. Flanagan, "Coding and use of tactile signals from the fingertips in object manipulation tasks." *Nat. Rev. Neurosci.*, vol. 10, no. 5, pp. 345–59, 2009.

[3] C. Piazza, G. Grioli, M. G. Catalano, and A. Bicchi, "A Century of Robotic Hands," *Annu. Rev. Control Robot. Auton. Syst.*, vol. 2, pp. 1–32, 2019.

[4] J. D. Madden, "Mobile robots: motor challenges and materials solutions," *Science*, vol. 318, no. 5853, pp. 1094–1097, 2007.

[5] S. Yang, J. Song, G. Li, W. Zhang, Z. Sun, D. Du, and Q. Chen, "Development of the ca robot finger with a novel coupled and active grasping mode," *Int. J. Humanoid Robot.*, vol. 13, no. 03, p. 1650012, 2016.

[6] C.-H. Xiong, W.-R. Chen, B.-Y. Sun, M.-J. Liu, S.-G. Yue, and W.-B. Chen, "Design and implementation of an anthropomorphic hand for replicating human grasping functions," *IEEE Trans. Robot.*, vol. 32, no. 3, pp. 652–671, 2016.

[7] M. Laffranchi, N. Boccardo, S. Traverso, L. Lombardi, A. Canepa, Michele a nd Lince, M. Semprini, J. A. Saglia, A. Naceri, R. Sacchetti, E. Gruppioni, and L. De Michieli, "The hannes hand prosthesis replicates the key biological properties of the human hand," *Sci. Robot.*, vol. 5, no. 46, p. eabb0467, 2020.

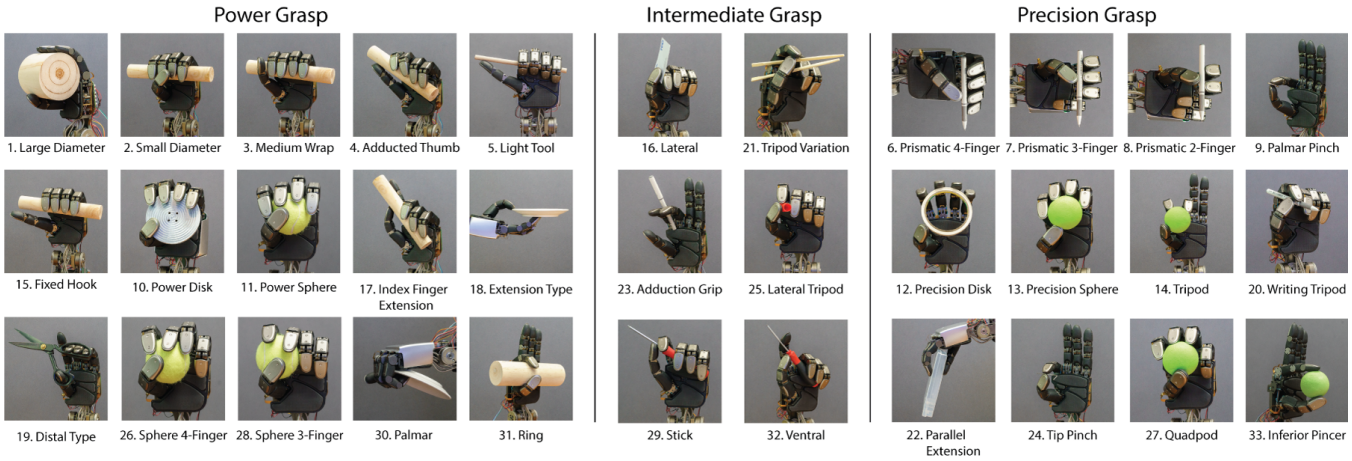

Fig. 11. Grasp taxonomy of TRX-Hand5. The poses and their indices correspond to the Feix Taxonomy [28].

[8] J. T. Belter, J. L. Segil, A. M. Dollar, and R. F. Weir, "Mechanical design and performance specifications of anthropomorphic prosthetic hands: a review," *J. Rehabil. Res. Dev.*, vol. 50, no. 5, pp. 599–618, 2013.

[9] S. C. Jacobsen, E. K. Iversen, D. F. Knutti, R. T. Johnson, and K. B. Biggers, "Design of the utah/m.i.t. dextrous hand," *Proc. IEEE Int. Conf. Robot. Automat.*, vol. 3, pp. 1520–1532, 1986.

[10] P. Tuffield and H. Elias, "The shadow robot mimics human actions," *Ind. Robot*, vol. 30, no. 1, pp. 56–60, 2003.

[11] H. Liu, K. Wu, P. Meusel, N. Seitz, G. Hirzinger, M. Jin, Y. Liu, S. Fan, T. Lan, and Z. Chen, "Multisensory five-finger dexterous hand: The dlr/hit hand ii," in *Proc. IEEE/RSJ Int. Conf. Intell. Robots Syst.*, 2008, pp. 3692–3697.

[12] D.-H. Lee, J.-H. Park, S.-W. Park, M.-H. Baeg, and J.-H. Bae, "Kitech-hand: A highly dexterous and modularized robotic hand," *IEEE/ASME Trans. Mechatron.*, vol. 22, no. 2, pp. 876–887, 2016.

[13] L. B. Bridgwater, C. A. Ihrke, M. A. Diftler, M. E. Abdallah, N. A. Radford, J. M. Rogers, S. Yayathi, R. S. Askew, and D. M. Linn, "The Robonaut 2 Hand – Designed to do work with tools," in *Proc. IEEE Int. Conf. Robot. Automat.*, no. September 2014, 2012, pp. 3425–3430.

[14] M. Grebenstein, M. Chalon, G. Hirzinger, and R. Siegwart, "Antagonistically driven finger design for the anthropomorphic DLR hand arm system," in *Proc. IEEE-RAS Int. Conf. Humanoid Robots*, 2010, pp. 609–616.

[15] Z. Kappassov, J. Antonio, C. Ramon, V. Perdereau, Z. Kappassov, J. Antonio, C. Ramon, and V. Perdereau, "Tactile sensing in dexterous robot hands – review," *Robot. Auton. Syst.*, vol. 74, no. A, pp. 195–220, 2015.

[16] H. Yousef, M. Boukallel, and K. Althoefer, "Tactile sensing for dexterous in-hand manipulation in robotics - A review," *Sens. Actuators A: Phys.*, vol. 167, no. 2, pp. 171–187, 2011.

[17] N. Jamali, M. Maggiali, F. Giovannini, G. Metta, and L. Natale, "A new design of a fingertip for the icub hand," in *Proc. IEEE/RSJ Int. Conf. Intell. Robots Syst.*, 2015, pp. 2705–2710.

[18] U. Kim, D. Jung, H. Jeong, J. Park, H.-M. Jung, J. Cheong, H. R. Choi, H. Do, and C. Park, "Integrated linkage-driven dexterous anthropomorphic robotic hand," *Nat. Commun.*, vol. 12, no. 1, p. 7177, 2021.

[19] H. Liu, K. Wu, P. Meusel, N. Seitz, G. Hirzinger, M. H. Jin, Y. W. Liu, S. W. Fan, T. Lan, and Z. P. Chen, "Multisensory Five-Finger Dexterous Hand: The DLR/HIT Hand II," in *Proc. IEEE/RSJ Int. Conf. Intell. Robots Syst.*, 2008, pp. 22–26.

[20] I. H. Taylor, S. Dong, and A. Rodriguez, "Gelslim 3.0: High-resolution measurement of shape, force and slip in a compact tactile-sensing finger," in *Proc. IEEE Int. Conf. Robot. Automat.*, 2022, pp. 10 781–10 787.

[21] J. W. James, A. Church, L. Cramphorn, and N. F. Lepora, "Tactile Model O: Fabrication and testing of a 3d-printed, three-fingered tactile robot hand," *Soft Robot.*, vol. 8, no. 5, pp. 594–610, 2021.

[22] H. Sun, K. J. Kuchenbecker, and G. Martius, "A soft thumb-sized vision-based sensor with accurate all-round force perception," *Nat. Mach. Intell.*, vol. 4, no. 2, pp. 135–145, 2022.

[23] H. Kawasaki, T. Komatsu, and K. Uchiyama, "Dexterous anthropomorphic robot hand with distributed tactile sensor: Gifu hand II," *IEEE/ASME Trans. Mechatron.*, vol. 7, no. 3, pp. 296–303, 2002.

[24] J. A. Fishel, V. J. Santos, and G. E. Loeb, "A robust micro-vibration sensor for biomimetic fingertips," in *Proc. IEEE RAS&EMBS Int. Conf. Biomed. Robot. Biomechatron.*, 2008, pp. 659–663.

[25] T. P. Tomo, A. Schmitz, W. K. Wong, H. Kristanto, S. Somlor, J. Hwang, L. Jamone, and S. Sugano, "Covering a robot fingertip with uSkin: A soft electronic skin with distributed 3-axis force sensitive elements for robot hands," *IEEE Robot. Autom. Lett.*, vol. 3, no. 1, pp. 124–131, 2017.

[26] M. T. Mason and J. K. Salisbury Jr, *Robot Hands and the Mechanics of Manipulation*. The MIT Press, Cambridge, MA, 1985.

[27] M. R. Cutkosky, "On grasp choice, grasp models, and the design of hands for manufacturing tasks," *IEEE Trans. Robot. Autom.*, vol. 5, no. 3, pp. 269–279, 1989.

[28] T. Feix, J. Romero, H.-B. Schmiedmayer, A. M. Dollar, and D. Kragic, "The grasp taxonomy of human grasp types," *IEEE Trans. Hum. Mach. Syst.*, vol. 46, no. 1, pp. 66–77, 2015.

[29] J. Krajbich, M. Pinzur, B. Potter, and P. Stevens, *Atlas of Amputations and Limb Deficiencies: Surgical, Prosthetic, and Rehabilitation Principles*, ser. AAOS - American Academy of Orthopaedic Surgeons. Wolters Kluwer Health, 2023.

[30] K. Matheus and A. M. Dollar, "Benchmarking grasping and manipulation: Properties of the objects of daily living," in *Proc. IEEE/RSJ Int. Conf. Intell. Robots Syst.*, 2010, pp. 5020–5027.

[31] Y.-J. Kim, Y. Lee, J. Kim, J.-W. Lee, K.-M. Park, K.-S. Roh, and J.-Y. Choi, "RoboRay hand: A highly backdrivable robotic hand with sensorless contact force measurements," in *Proc. IEEE Int. Conf. Robot. Automat.*, 2014, pp. 6712–6718.

[32] A. Schmitz, U. Pattacini, F. Nori, L. Natale, G. Metta, and G. Sandini, "Design, realization and sensorization of the dexterous icub hand," in *Proc. IEEE-RAS Int. Conf. Humanoid Robots*, 2010, pp. 186–191.

[33] S. Standring, *Gray's Anatomy: The Anatomical Basis of Clinical Practice*. Am Soc Neuroradiology, 2005.

[34] P. Lu, J. Liang, B. Huang, S. Yang, and W. W. Lee, "Thermoformed electronic skins for conformal tactile sensor arrays," in *Proc. IEEE Int. Conf. Robot. Automat.*, 2024, accepted.

[35] F. Bergner, E. Dean-Leon, and G. Cheng, "Design and realization of an efficient large-area event-driven e-skin," *Sensors*, vol. 20, no. 7, pp. 1–33, 2020.

[36] A. Kapandji, "Cotation clinique de l'opposition et de la contre-opposition du pouce," in *Annales de Chirurgie de la Main*, vol. 5, no. 1. Elsevier, 1986, pp. 67–73.